materials

MDPI

Article

Preparation and Optimization of Fluorescent Thin Films of Rosamine-SiO_2/TiO_2 Composites for NO_2 Sensing

María G. Guillén [1], Francisco Gámez [1], Belén Suárez [1], Carla Queirós [2], Ana M. G. Silva [2], Ángel Barranco [3], Juan Ramón Sánchez-Valencia [3], José María Pedrosa [1] and Tânia Lopes-Costa [1,*]

1 Departmento de Sistemas Físicos, Químicos y Naturales, Universidad Pablo de Olavide, Sevilla 41013, Spain; mariagonzalez88@gmail.com (M.G.G.); fgammar@gmail.com (F.G.); bsuarezjimenez@yahoo.es (B.S.); jmpedpoy@upo.es (J.M.P.)

2 REQUIMTE-LAQV, UCIBIO Departamento de Química e Bioquímica, Faculdade de Ciências da Universidade do Porto, R. Campo Alegre, Porto 4169-007, Portugal; up199800393@fc.up.pt (C.Q.); ana.silva@fc.up.pt (A.M.G.S.)

3 Instituto de Ciencia de Materiales de Sevilla, Universidad de Sevilla-CSIC, Américo Vespucio 49, Sevilla 41092, Spain; angel.barranco@csic.es (Á.B.); jrsanchez@csic.es (J.R.S.-V.)

* Correspondence: tlopcos@upo.es; Tel.: +34-954-977-363

Academic Editor: Shlomo Berger

Received: 7 December 2016; Accepted: 23 January 2017; Published: 31 January 2017

Abstract: The incorporation of a prototypical rosamine fluorescent dye from organic solutions into transparent and microstructured columnar TiO_2 and SiO_2 (MO_2) thin films, prepared by evaporation at glancing angles (GAPVD), was evaluated. The aggregation of the adsorbed molecules, the infiltration efficiency and the adsorption kinetics were studied by means of UV-Vis absorption and fluorescence spectroscopies. Specifically, the infiltration equilibrium as well as the kinetic of adsorption of the emitting dye has been described by a Langmuir type adsorption isotherm and a *pseudo*second order kinetic model, respectively. The anchoring mechanism of the rosamine to the MO_2 matrix has been revealed by specular reflectance Fourier transform infrared spectroscopy and infiltration from aqueous solutions at different pH values. Finally, the sensing performance towards NO_2 gas of optimized films has been assessed by following the changes of its fluorescence intensity revealing that the so-selected device exhibited improved sensing response compared to similar hybrid films reported in the literature.

Keywords: rosamine dyes; porous columnar semiconductors; gas sensors

1. Introduction

Xanthene dyes comprise a set of molecular architectures that possess particularly efficient absorptive and fluorescence properties. In combination with specific singularities acquired upon selective functionalization of the xanthene moiety, their applications have been progressively extended among a large landscape of technological areas [1–6]. For instance, the sensitizing effect provoked by the environment in rhodamine fluorophores has been widely employed as part of hybrid materials in fields as dye sensitized solar cells or chemosensing [7–11]. Moreover, their intense fluorescence emission allows their use as fluorescent probes, laser dyes, pigments, fluorescent standards or detection of reactive organic species [12–15]. These molecules are also widely used in biotechnology—for example, in the study of the membranes fluidity, the structure and dynamics of micelles, imaging in cells, and also in sensors for the detection of mercury, copper, iron and chromium in cells [16–19].

Although for some of these applications the dye is used in solution, most of them require this fluorescent probe to be anchored to a solid surface [20–26]. From a molecular viewpoint, establishing optimal values for the dye concentration, pH and solvent will determine the dominant chemical forms in the equilibrium, where cationic, zwitterionic, covalent dimers and π-π aggregates can exist. However, despite these cautions, when transferring to a solid matrix, the external potential represented by the solid walls in its pores makes the dyes even more prone to aggregation. This aggregation-inductive effect strongly challenges some practical goals by masking their solution-optimized emission properties when transferred to a rigid substrate. In this direction, materials science put at our disposal a wide plethora of functionalized substrates with predefined compositions and micro and nanostructures that present the adequate optical and electronic properties for very specific applications [27–38]. Remarkably, physical vapor deposition (PVD) methods allow us a very subtle and independent control of the structural and morphological parameters of the films, becoming an appropriate choice for the fabrication of hybrid materials [39]. Specifically, glancing angle physical vapor deposition (GAPVD) generates mainly columnar structures with micro and mesostructured porous surfaces [40–43] very suitable for the infiltration and incorporation of active molecules into photonic devices.

Additionally, since the core of these rhodamine dyes is constituted by a planar xanthene ring 3,6-disubstituted by in-plane amino groups and a nearby perpendicular 2′-carboxyphenyl ring in position 9, a pH-dependent behavior of the optical properties emerge as a consequence of the equilibrium between a fluorescent open ring and a non-fluorescent spirolactone forms [44]. Hence, in some circumstances, this feature goes hand-in-hand with the steric hindrance of the ring that preserves the anchoring to the substrate by the carboxylic substituent. Transposition of the carboxylic group from the 2′ to the 4′ positions suppresses these effects to a large extent. The resulting ensemble of molecules obtained within this positional change is denominated rosamine and its optimized synthetic procedure has been reported elsewhere [45]. The similarities between rhodamines and rosamines make them candidates for similar applications avoiding the mentioned chemical challenges.

An innovative aspect of the present work is the coupling of both aspects by incorporating the rosamine shown in Figure 1 into non-dispersive TiO_2 and SiO_2 thin films prepared by GAPVD as hosting matrices. Taking into account the chemical structure of this rosamine, it can be anchored to the MO_2 surface by electrostatic interaction between its ammonium group and the negatively charged surface of the oxide, or by chemical binding through its carboxylic group (well known in the field of dye sensitized solar cells). The spectroscopic properties of the films and the thermodynamics and kinetics of the dye incorporation process were evaluated. Their fluorescence response will be finally tested for the case of the best-behaved composite against the toxic NO_2 gas which constitutes a very dangerous air pollutant for both environmental and human health [46].

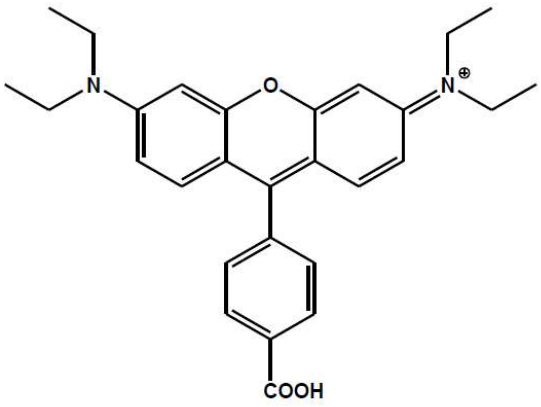

Figure 1. Schematic structure of the rosamine B molecular ion.

2. Results and discussion

2.1. Spectroscopic Characterization of RosB/MO_2 Composites: Molecular Aggregation

The RosB absorption spectrum in CH_2Cl_2 is constituted by a monomer band at 564 nm and a vibronic shoulder (traditionally called dimer band) at 527 nm (see Figure S1 in the Supplementary Material Section). The difference in the monomer-dimer absorbance peaks is consistent with their rhodamine fluorophore analogue [47]. Prior to further measurements, the use of CH_2Cl_2 is justified here because, besides presenting a positive solvatochromic effect that is not of interest for this work, it disfavors the aggregation with respect to aqueous solutions, mainly due to the smaller dielectric sandwiching effect and the absence of intermolecular hydrogen bonding in the former solvent. This fact is clearly shown in Figure S1 in the Supplementary Material section, where the absorbance spectra of a diluted solution of RosB in water and in organic CH_2Cl_2 solvents are compared.

The higher value of the aggregate/monomer *ratio* in the aqueous solution is apparent as expected. However, considering that the shape of the excitation spectra was always found to be very similar to that of their absorption spectra, this fact has been understood as the existence of a single type of molecules/aggregates with a spectrum characterized by two bands. These bands occur at shorter and longer wavelengths in relation with the maximum absorption of the monomer and are labeled as *H* and *J* bands, respectively [10]. An additional interpretation to this phenomenon can be mentioned: the aggregates can produce a similar emission to that of the monomers.

Regardless of the specific choice for the interpretation of the data, changes in the absorption profile can be unequivocally attributed to different ensembles of supramolecular arrangements. Hence, we will keep the classical first order exciton theory (ET) for the explanation of the experimental evidence. In this theory, these bands are attributed to the absorption of the dyes in dimeric forms with different mutual orientations labeled also as *H* and *J* (or Scheibe) dimers. These preformed aggregates play an important role in the emission properties of the supported composite. It is reported that dimers constitute efficient non radiative quenchers of the fluorescence by an internal conversion from charged-transfer states in their fundamental ground to excited singlet followed by an intersystem crossing to the charge-transfer triplet states [48]. In the way the preformed aggregates (mostly dimers) contribute to the total quenching upon deposition, it will be a factor to take into account in the choice of the optimum conditions for the highly emitting devices stated in the title. Although the Stokes shift (i.e., the difference between the maximum wavelengths of absorbance and fluorescence) clearly increases with RosB concentration (see Figure S2), no appreciable shape changes appear in the absorption spectrum of RosB in CH_2Cl_2 within the concentration range explored in this study. This fact ascribed to reabsorption phenomena has been described in dyes with overlapping emission/absorption spectra due to the absence of dipole moment parallel to the long axis [49]. In any case, the quenching of the fluorescence emission with the dye concentration shows a well-defined behavior that could be visualized by means of the ratio between the fluorescence intensity and the absorbance at the excitation wavelength (fluorescence efficiency) as shown in Figure S3. In view of the comments that we have given above, this diminution in solution cannot be associated to an enhancement of the aggregation but to reabsorption.

In Figure 2, the absorption spectra of the RosB infiltrated in MO_2 films at an infiltration time of 24 h from different bulk concentrations is compared with the spectra of the CH_2Cl_2 solution at 3.5 μM for the sake of visual facilitation, considering that no appreciable aggregation contribution to the total amount of molecules in organic solution was observed. A general aspect of the adsorbed rosamine spectrum is that the absorption bands are broadened because of the interaction with the inorganic matrix and the formation of *H* aggregates as revealed by the progressive growth of the shoulder at ~527 nm with the concentration of the RosB in the infiltrating solution. The stacking of RosB into non-covalent complexes is enhanced in TiO_2 as observed in the comparison of both panels of Figure 2 as a consequence of the influence of the environment micropolarity and microacidity. This occurrence can be attributed to the higher acidic character of the surface hydroxyl groups in

silanol with respect to titanol and to the charge compensation process that is the leading contributing effect to self-aggregation. Given the similarities with rhodamine B, rosamine B should own a pK_a value of ~3 [50]. A zwitterionic form is then expected in this solvent allowing for a one- or two-sided anchoring to the surface charges of the matrices. Nevertheless, the point of zero charge (*pzc*) differs from ~2.4 for SiO_2 to ~5.5 for TiO_2 [43,51], and, hence, the charge balance between MO_2 and the zwitterionic form of RosB would be differently equilibrated in the matrices, and the anchoring will also be unlike between them. This aspect will be discussed below by means of vibrational spectroscopy and infiltration of the matrices with aqueous solutions at different pH values.

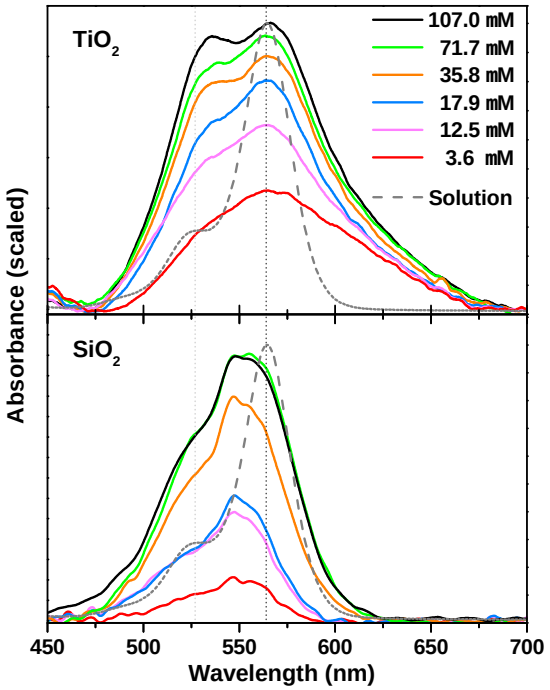

Figure 2. Absorption spectra for composite RosB/MO_2 thin films prepared by infiltration of CH_2Cl_2 solutions at different concentrations. The infiltration time was 24 h in all cases. The corresponding spectrum in solution is plotted as dashed lines for the sake of comparison.

In the limit of the diluted dye concentration, a broad distribution at longer wavelengths clearly emerges upon adsorption, which, according to ET, can be attributed to head-to-tail *J*-aggregates. The relative monomer/oligomer population decreases when the concentration increases (metachromatic effect) and also broadens and shifts to shorter wavelengths, which, provided π interactions with the free electrons of oxygen atoms in the surface are of minor importance in non-doped oxides [52], is indicative of an augmentation of the aggregation number of non-fluorescent sandwich-like *H*-aggregates.

Additionally, the blueshift of the monomer band in SiO_2 (547 nm) is indicative of a more basic character of the environment created by the residual silanol groups and non-interacting amino groups within the pores of the amorphous silica columns with respect to the CH_2Cl_2 solution [53]. Remarkably, this band seems to have acquired a more structured shape with a new band at 555 nm. We tentatively assigned this feature to the existence of micro and mesoporous in the nanocolumns that will be detailed further along in this discussion. A plausible contribution to the splitting in the energy levels of the protonated and zwitterionic forms of the dye that are usually ill-resolved should also be mentioned [54]. *H*-dimerization is less accentuated, and a smaller aggregation number can be inferred from the nearly constant frequency of the dimer band. Therefore, a priori, rosamine infiltrated in SiO_2 will provide better results in relation with its photoluminescence efficiency properties despite it throwing smaller absorbance intensity in comparison with TiO_2 because the rosamine load is also smaller in these samples. These aspects are treated in detail in the following.

2.2. Spectroscopic Characterization of RosB/MO_2 Composites: Adsorption Equilibrium and Kinetics

Adsorption isotherms have been derived from the above results. The absorption band is integrated as a measure of the total amount of RosB molecules attached to MO_2, i.e., the molecular surface concentration Γ [55]. The experiments were carried out by infiltrating RosB into the films during 24 h for a set of dye solutions with different concentrations as shown in Figure 3. The shape of the measured data indicates a high increment for small RosB concentrations to reach a high value at a solution concentration of around 40 μM and saturation is reached for more concentrated solutions. The so-obtained data are fitted to a Langmuir function of the form:

$$A = \frac{C_L b[\text{RosB}]}{1 + b[\text{RosB}]}, \tag{1}$$

where A represents the integrated absorption band. The additional C_L and b parameters stand for the adsorption capacity and affinity parameter in the Langmuir model. It should be mentioned that the fitting to Freundlich, Dubinin–Radushevich or Temkin models does not result in such an accurate reproduction of these points ($R^2 \geq 0.99$). The obtained parameters would put in front of the optimum performance for sensing to nanocolumnar TiO_2 films, with a double number of adsorption sites and a higher affinity of the dye (in a factor 6 with respect to SiO_2). However, most parts of the absorption band in TiO_2 is due to non-fluorescent *H*-aggregates, and, hence, a notable quenching of the fluorescence properties will dominate these composites as we have commented on above.

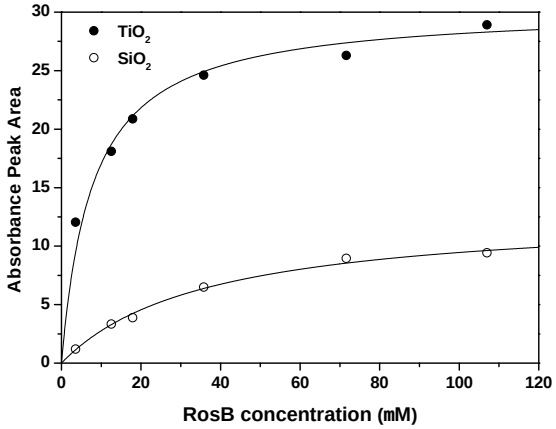

Figure 3. Adsorption behavior for RosB infiltrated in MO_2 films. The corresponding fit to a Langmuir-type function is denoted with a continuous line while experimental data are labeled with circles.

The temporal behavior of the infiltration of the dye molecules into the columnar MO_2 films has also been studied. The obtained experimental data is divided into a fast growth followed by a much slower process while approaching a saturation value Γ_∞ (see Figure S4 in the Supplementary Material section). This pattern can be adjusted with the pseudosecond order adsorption kinetics model that has been tested for chemisorption of dyes into inorganic matrices [56], and it is supposed to account for the surface chemical bonds and physical diffusion steps. The model is the result of solving the following rate equation:

$$\frac{d\Gamma(t)}{dt} = k_2[\Gamma_\infty - \Gamma(t)]^2 \tag{2}$$

that can be straighforwardly integrated with the appropriate boundary condition ($\Gamma(0) = 0$) to get:

$$\frac{1}{\Gamma_\infty - \Gamma(t)} = \frac{1}{\Gamma_\infty} + k_2 t, \tag{3}$$

with k_2 the pseudosecond order adsorption rate. This equation can be linearized in several ways, and we have chosen [57]:

$$\frac{t}{A(t)} = \frac{1}{k_2 A_\infty^2} + \frac{1}{A_\infty} t \quad (4)$$

by considering again that the integrated absorption band A is proportional to Γ.

The result is plotted in Figure 4 for the 35.8 μM solution in the whole time range considered, with $R^2 \geq 0.999$. Similar fitting parameters are obtained for the two matrices, with (A_∞, k_2) = (25.3, 0.0042) and (22.6, 0.0038) for TiO_2 and SiO_2, respectively, in units of [A_∞] = nm and [k_2] = min^{-1}. Together with the Langmuir fitting, it implies that these MO_2 columnar microstructures exhibit a good infiltration capacity but also an excellent surface functionality for chemical adsorption and a good porous structure for the diffusive accessibility of the incoming rosamine molecules to the active adsorption sites.

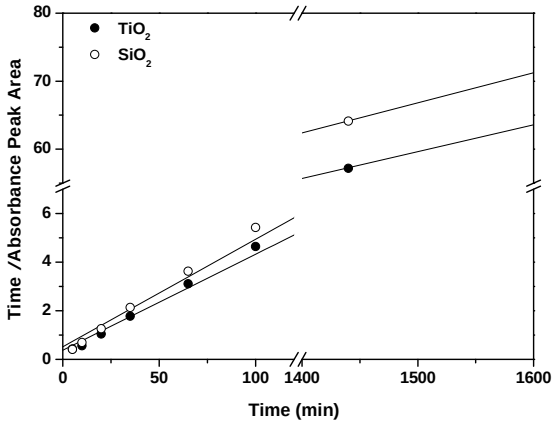

Figure 4. Linearized plot of the temporal evolution of the adsorption of RosB molecules infiltrated in MO_2 films. The corresponding fit is denoted with a continuous line while experimental data are labeled with circles.

2.3. Spectroscopic Characterization of RosB/MO_2 Composites: Anchoring

As mentioned above, the molecular structure of RosB enables its anchoring to MO_2 by chemical (through the carboxylic group) or electrostatical (through the amonium group) bounds. In Figure 5, the specular reflectance Fourier Transformed Infrared (FTIR) spectra of RosB and MO_2 precursors have been compared with the bounded RosB in order to analyze the spectral changes in the region of the carbonyl and hydroxyl groups. Only the RosB bands with a major percentage (more than 50%) of potential energy distribution of normal modes of vibration located in the ethylamine (A), phenyl ring with the COOH group (P) or xanthene ring (X) groups are labeled according to the assignment reported in Ref. [58]. First of all, the strong absorption of the M-O-M asymmetric (transverse-optic and longitudinal-optic modes) stretching band clouds the signals coming from bounded RosB and hence this region is shadowed in the figure. In the 3300–3900 cm^{-1} region, there is the superposition of the hydrogen bond network of silanol and titanol groups and to the symmetric and antisymmetric OH modes of water coordinated to M^{4+} cations [59]. Finally the bending motion of the adsorbed H_2O molecules appears at ∼1640 and ∼1710 cm^{-1} for TiO_2 and SiO_2, respectively [60,61]. The comparison of the RosB precursor with the bounded RosB spectra sheds light on to the mechanistic pathway of its surface anchoring. In the SiO_2 substrate, the bands associated with the amine modes (A) disappear, at least partly, while the shape of the OH region remains unaltered with respect to the untreated substrate. This fact indicates an electrostatic anchoring of RosB to SiO_2 and is in agreement with the absence of solid data supporting chemical bounds in carboxylic-dyes attached to silica matrices. On the contrary, in TiO_2, both types of bands (A and P) suffer modification upon adsorption. Particularly, the bands

at ~1490, ~1400 and ~1180 cm^{-1} that are assigned to C=O, C-O and C-OH vibration become much weaker in favor of two new bands (marked with an asterisk) that correspond to the symmetric and asymmetric CO_2^- vibrations. These changes in the bands associated to P-vibrations have been reported to be compatible with chelating and/or bidentate binding modes of the carboxylate groups on the TiO_2 surface. Overall, it seems plausible that RosB is anchored to TiO_2 by two different ways: electrostatic or chemical bounds, which would explain the higher load derived for these films from Figure 3.

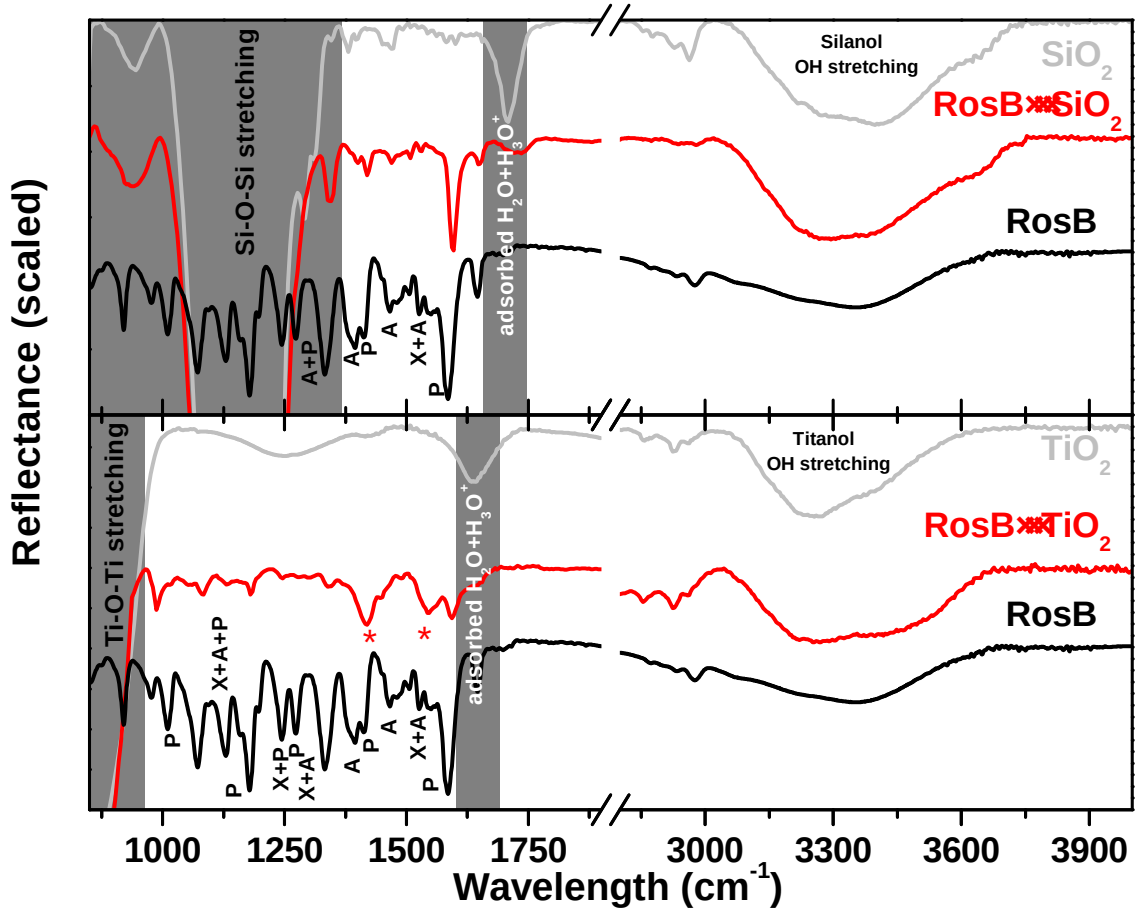

Figure 5. Specular reflectance Fourier Transform infrared spectra of MO_2 and RosB precursors compared with the bounded RosB$\cdots MO_2$ in the devices. Vibration bands associated with phenyl ring (P). Amine (A) and xanthene ring (X) are indicated conveniently. See the main text for details.

Complementary information can be extracted by infiltrating the dye from aqueous solutions at different pH values as reported in Figure S4 (Supplementary Information Section). The charge compensation on the inorganic matrix surface will depend on its *pzc* as explained above. In this sense, the immersion of a solution with a pH higher than its *pzc* results in a net negative charge on its surface by dissociation of the -OH (titanol or silanol) surface groups that is compensated by the cations in the double layer. With this point in mind and taking into account the pK_a value of the RosB molecule, in SiO_2, the maximum load is reached for the measured pH which is closer to the pK_a. If appreciable contribution of chemical anchoring takes place in these substrates, a much more evident increase near the point of charge compensation between RosB and MO_2 would be seen. This is the case of TiO_2 where the dye load is significantly enhanced near its *pzc* value and decreases with the pH because a deficient charge compensation of the excessive negative charge on the surface, i.e., the net negative charge in the surface is partly compensated by the positive charge of the zwitterionic RosB, but the

overall charge remains negative, a fact that makes difficult a new approaching of another dye molecule. Thus, it is reconfirmed that while in TiO_2 the anchoring occurs *via* chemical and electrostatic bonding, and this is not the case in SiO_2 where an electrostatic mechanism seems to dominate the adsorption of RosB.

2.4. Photoluminescence of RosB/MO_2 Composites: Choosing the Optimal Preparation Conditions for Enhancing the Fluorescence Signal

As it has been discussed in the previous sections, whereas both monomers and aggregates are active in absorption, only the lowest excited state of dimers (the *J* dimers) and the monomers are fluorescent. Specific *J*-*H* conversion would require the measurement of fluorescence life times and is out of the scope of the present work. Fluorescence spectra constitute a mapping of (mainly) the monomeric state emission without the influence of the *H*-dimers and higher order aggregate quenching. Having this idea in mind, the interpretation of the temporal evolution of the infiltrated rosamine in MO_2 presented in Figure 6 is eased. For the assistance of the subsequent explanation, the corresponding wavelength of the maximum fluorescence (589 nm) of the RosB monomer (3.5 μM) in CH_2Cl_2 solution is presented as a vertical line. This figure shows the temporal evolution of the RosB fluorescence infiltrated from two different concentration solutions in the two oxides. In both SiO_2 and TiO_2 films, the intensity evolution with infiltration time follows the same trend. The rosamine molecules infiltrated from a diluted solution increase their fluorescence intensity with time as a consequence of the smaller aggregation rate. If the concentration of the infiltrating solution is increased, the *H*-aggregation is apparent in the diminution of the intensity with the infiltration time in comparison with the diluted case, i.e., the emission is quickly quenched with infiltration time. This is also supported by the results shown in Figure 2. However, even when the fluorescence of SiO_2 films is smaller than those obtained for TiO_2 films, the first owns a comparably smaller loading capacity with respect to TiO_2 as extracted with the corresponding Langmuir fitting. This point holds for both RosB concentrations with higher emission capacity for SiO_2, again related to the lower rosamine aggregation observed in this material when compared to TiO_2 (see Figure 2). Therefore, the films with the optimum optical properties are those constituted by a solid nanocolumnar SiO_2 infiltrated with diluted RosB solution that exhibit the higher emission capacity in relation with the number of adsorbed molecules. It seems timely to mention that higher exposition times ($\geq$24 h) lead to a diminution of the intensity even in the diluted cases because aggregation started to grow even in the open and wide mesoporous of their external surface.

The spectral details observed in the four cases can be explained by the opposing effects of aggregation and structural allocation of the dye. While *J*-aggregation induces a redshift of the photoluminescence bands, the fluorescence of the dye monomers adsorbed on different areas of the MO_2 structure also provokes a shift evolution from monomers infiltrated to the inner parts or micropores of the oxide to a blue-shifted peak near to the solution maximum that corresponds to the outer-placed monomers. The same effect has been described in dyes adsorbed in different smectite (clay) minerals [62,63] in which the fluorescence of the adsorbed molecules at the external surface of smectites occurs at a lower wavelength than the corresponding fluorescence of Rhodamine 6G in the interlamellar space. This effect seems to be due to a geometrical constraint caused by the restricted space that reinforces the π-delocalization between both chromophores by a conformational-locking in which a more parallel disposition of the phenyl ring respect to the xanthene plane is favored [64]. Additional contributions of the microenvironment changes cannot be ruled out but do not explain the observed changes by themselves. In both MO_2 films, the fluorescence intensity in the concentrated cases diminishes as a consequence of the *H*-aggregation, while *J*-aggregation induces a redshift with infiltration time as commented above. The structural effects of the inorganic matrix is negligible in these cases due to the high number of molecules filling the pores. In TiO_2, we found a slight shift to the blue with infiltration time for the diluted RosB solution as a result of the adsorption from the inner (microporous) to the outer surface as it can be deduced from the closeness of the

maximum fluorescence intensity with respect to the monomer emission in solution. The absence of a heterogeneous distribution of pores in SiO_2 is the reason behind the redshift in the diluted case which can be attributed to *J*-aggregation as in the concentrated counterpart.

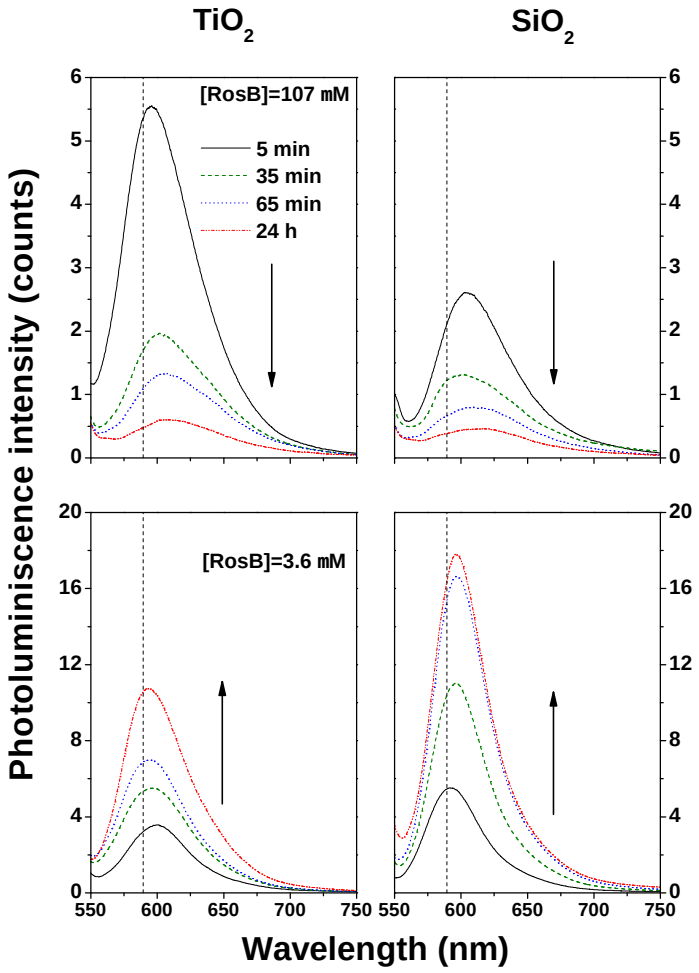

Figure 6. Photoluminescence spectra for composite RosB/MO_2 thin films prepared by infiltration of dichloromethane solutions at the highest and lowest concentrations considered at different infiltration times.

2.5. Sensing Response to NO_2 Gas

As a final application of the selected SiO_2 microfilms infiltrated with diluted rosamine solution, we have tested the spectral changes provoked by an exposure to a NO_2 stream (50 ppm). The observed spectral changes upon NO_2 exposure documented in the top panel of Figure 7 ($\Delta\lambda$ = 11 nm) demonstrate that rosamines bounded to a solid matrix constitute a good choice for gas detection. The most probable mechanism for such changes is possibly an oxidation reaction through a charge transfer process from the electron-rich xanthene ring to the oxidant gas [65–67]. Although the observed bathochromic shift is independent from the RosB concentration of the infiltrated solution, the intensity drop decreases with this concentration. For instance, the decrement of 23% observed for the most diluted solution is only 9% when the RosB concentration is quintupled (data not shown). This difference can be clearly explained in terms of the different aggregation state of the RosB molecules in these films: while low aggregation facilitates the analyte penetration and interaction, high molecular aggregation prevents this process [68]. The situation is even clearer when the more sensible fluorescence is tested

as a sensing parameter, while, in the selected film with low aggregation state, the intensity falls off up to 84% and this drop is only of about 37% for a film infiltrated with a 36 μM solution.

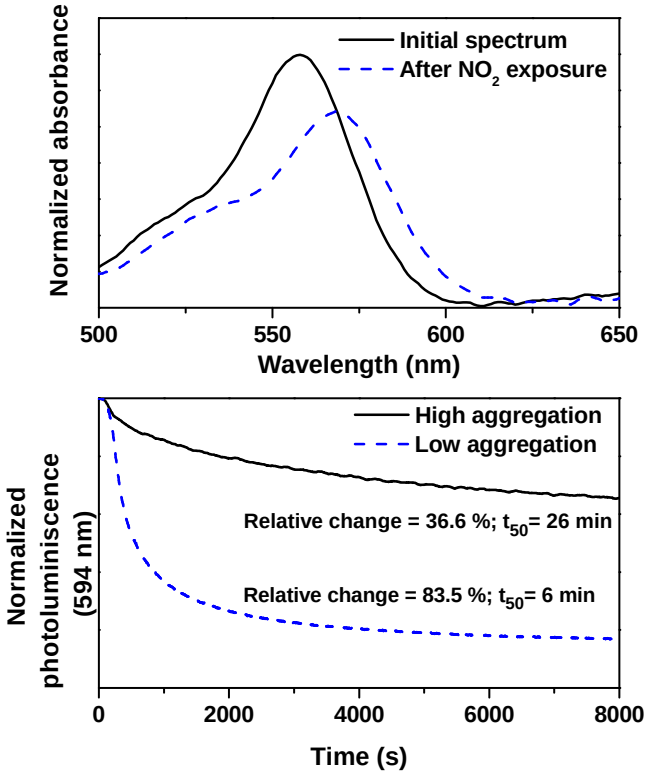

Figure 7. Top panel: spectral changes of the visible absorption spectrum of RosB (3.6 μM) bounded to SiO_2 before and after NO_2 (50 ppm) exposure. Bottom panel: photoluminescence response to NO_2 (50 ppm) of RosB infiltrated in SiO_2. The continuous line corresponds to 36 μM concentration (highly aggregated solution) and the dashed-lines stand for the 3.6 μM solution infiltration.

The speed of the response is evaluated with the t_{50} parameter, i.e., the time taken for the photoluminescence to reach 50% of its minimum value after NO_2 exposure. The obtained value (6 min) is reasonably low and smaller than those obtained in recent porphyrin-based sensors (10.3 min) [69], thus confirming the fast response of SiO_2. Conversely, the values of the t_{50} increases up to 26 min for the aggregated case in SiO_2 and is even higher in the TiO_2 films with significantly reduced intensity changes. The higher aggregation in these latter samples precludes their use as gas sensors [68]. Additionally, only partial reversibility is reached after a recovery phase employing N_2 while heating the samples. The concentration dependence of this response will be treated in a future work.

3. Conclusions

In the present work, the incorporation of a rosamine into transparent and microstructured columnar TiO_2 and SiO_2 thin films prepared by GAPVD have been investigated. The resulting composites exhibit low refractive indexes, high porosity, controlled thicknesses and robustness that, together with their spectroscopical properties, are judged as appropriate for photonic-based devices.

The concentration and time dependence of the infiltration process have been followed by spectroscopic measurements, and the results can be well described by a Langmuir and a *pseudo*second order kinetics for the equilibrium and adsorption kinetic, respectively, discarding the physical diffusion to active adsorption sites as a limiting step in the dye infiltration. The spectroscopic features make evident that the aggregation rate is much more pronounced when the infiltration takes place from a concentrated solution and also in TiO_2 films. The compensation of charges is different in the

substrates because of their *pzc*, and, in consequence, the anchoring of the dye will also be different as demonstrated by FTIR. Therefore, a decrease in the fluorescence of the films with concentration and with infiltration time is the normal trend except for MO_2 films infiltrated with a diluted RosB solution, in which the infiltration time also causes an increase of the fluorescence. Taking the absolute value of the emission intensity as the property of interest, the SiO_2 film was tested as a NO_2 sensor, indicating that the film response is fast and suitable for gas detection.

The strong influence of the interaction of the dye with the inorganic host has prompted us to perform experiments on different substrates that disfavor the *H*-aggregation into its surface and thus increase the sensoring response upon exposure to specific analytes [70]. Some preliminary advances on sinthered anatase TiO_2 seem to be very promising and will be the topic of a future publication.

4. Materials and Methods

4.1. Chemicals

The synthesis of the xanthene dye [9-(4-carboxyphenyl)-6-diethylamino-3-xanthenylidene]-diethylamine chloride is fully described elsewhere [45]. Briefly, its synthesis involves a two-step sequence: (1) the microwave-assisted condensation of 3-(diethylamino)phenol with formylbenzoic acid in water and (2) oxidation with chloranil, followed by a chromatographic purification. The final molecular structure constitutes a positional isomer of rhodamine B, and, hence, it will be denoted as rosamine B (RosB) henceforth. Its optical properties in dichlorometane are also quite similar to those of rhodamine B [45], but the extinction coefficient at maximum absorption is only one-third of the rhodamine value. Dichlorometane was supplied by Sigma-Aldrich (Madrid, Spain) and was used as received.

4.2. Fabrication of MO_2 Films and RosB Infiltration

Composite RosB/SiO_2 and RosB/TiO_2 thin films were prepared by using porous SiO_2 and TiO_2 thin films as inorganic host matrices. This matrices will be denoted as MO_2 henceforth. The transparent (nondispersive) and amorphous TiO_2 and SiO_2 columnar films were prepared by the GAPVD technique at room temperature at an angle of deposition of 70° with respect to the evaporation source. The microstructure of the films is evaluated by field emission scanning electron microscopy. Concretely, the angle formed by the columns and the substrate was approximately 60°, with a film thickness of approximately 350 nm. The mesostructure of the films is characterized by exhibiting a high porosity as determined by measuring the adsorption of water with a quartz crystal monitor corrected with the mass thickness of the thin film as determined by both Rutherford backscattering and X-ray fluorescence analysis (total pore volume of 49% in case of TiO_2 films and 35% in case of SiO_2 films). Therefore, coupled with electronic microscopies analysis, void apertures on the surface in the form of micropores (pore diameter $\leq$ 2 nm) in TiO_2 and both micro and mesopores (pore diameter $\geq$ 2 nm) in SiO_2 are observed. This feature would allow the accessibility of the rosamine during the composite film preparation and the NO_2 molecules during the gas sensing experiments. The high porosity of the films also determines a refractive index value. By using absorption spectroscopy that was found to be relatively low (1.79) in the case of TiO_2 films [71] and very low (1.317) in the case of SiO_2 films [10], allowing their use in UV-Vis measurements. Further details regarding film preparation, SEM images and structural information can be found elsewhere [10,72]. For specular reflectance Fourier transform infrared (FTIR) spectroscopy, the films were deposited on gold-coated silicon substrates, whereas films for UV-Visible spectroscopy were prepared on glass substrates.

Binding of rosamine to the TiO_2 and SiO_2 films were performed by immersion of the substrates in several dichloromethane solutions of the dye. Afterwards, the films were rinsed with dichloromethane to remove dye molecules that were not incorporated into the film, and dried in air. Prior to the measurements, all films were cleaned with a dry N_2 stream.

4.3. Instrumentation

UV-Visible absorption spectra were recorded using a Cary 100 UV-Vis spectrophotometer (Agilent, Madrid, Spain). Photoluminescence spectra and sensing kinetics were recorded with a Hitachi F-7000 Fluorescence Spectrophotometer (Hitachi High Technologies, Krefeld, Germany). For exposures to NO_2, RosB/MO_2 films were placed in a purpose-modified sealable fluorescence cuvette with a gas inlet and an outlet. Two Bronkhorst F-201FV mass flow controllers (Bronkhorst High-Tech BV, Ruurlo, The Netherlands) were used to control the flow rates of gases. Dry N_2 was flowed into the cuvette before introducing the sample in order to remove any possible contaminating gases. After placing the sample in the cuvette, a constant dry N_2 flow was kept to protect it during thermal stabilization. A constant flow of NO_2 (50 ppm) was obtained from a cylinder from Abelló-Linde (Cádiz, Spain) Linde and introduced into the cuvette until complete saturation of the RosB. Samples were exposed at room temperature. Finally, dry N_2 was made to flow into the cuvette during the recovery stage.

Specular reflectance FTIR spectroscopy experiments in RosB/MO_2 films were performed using a Bruker IFS 66/S spectrometer (Bruker, Madrid, Spain). The background signal obtained from a gold substrate was subtracted in all cases. The infrared spectrum of rosamine B powder was measured in attenuated total reflectance (ATR) mode in a Jasco FT/IR-4100 espectometer (Jasco Inc., Easton, PA, USA) in an ATR Pro One module with an incidence angle of 45°. All spectra were obtained using typically 200 scans with a resolution of 4 cm^{-1}.

Supplementary Materials: The following are available online at www.mdpi.com/1996-1944/10/2/124/s1. Figure S1: Normalized absorption spectra of RosB in dichloromethane and water solutions at a 3.5 μM concentration, Figure S2: Concentration dependence of the photoluminescence spectra of RosB in dichloromethane. The absorption spectra of the most diluted solution is shown for the sake of comparison. The Stokes's shift in the photoluminescence spectra with the dye concentration is due to reabsortion phenomonema as explain in the main text, Figure S3: Emission capacity of the RosB in dichlorometane solution as a function of the concentration. The quenching of fluorescence can be attributed to reabsortion phenomena, provided the negligible effect of the dye concentration in the absorption spectra, Figure S4: Temporal evolution of the adsorption of RosB molecules infiltrated in MO_2 films, Figure S5: Evolution of the absorption band as a function of the pH during the infiltration procedure in MO_2 substrates from aqueous solutions.

Acknowledgments: The Oporto group thanks Fundação para a Ciência e a Tecnologia (FCT/Ministério da Ciência, Tecnologia e Ensino Superior) for the financial support to the UID/MULTI/04378/2013-POCI/01/0145/FERDER/007728 (Research Unit on Applied Molecular Biosciences, UCIBIO/ Rede de Química e Tecnologia, REQUIMTE), UID/QUI/50006/2013- POCI/01/0145/FERDER/007265 (Laboratório Associado para a Química Verde/REQUIMTE) through national funds and co-financed by the Fondo Europeo de Desarrollo Regional (FEDER), under the PT2020 Partnership Agreement, and to the project M-Era-NET/0005/2014. The group from Sevilla gratefully acknowledges funding from the Ministry of Economy and Competitivity (MINECO) under Projects MAT2014-57652-C2-2-R and PCIN-2015-169-C02-02 (under the project M-Era-NET/0005/2014). Funding from the Operative Programme FEDER-Andalucia through project P12 FQM-2310 also contributed to the present research.

Author Contributions: J.M.P. and T.L.-C. conceived and designed the experiments; M.G.G. and B.S. performed the sensing experiments; J.R.S.-V. and A.B. did the semiconductors films, C.Q. and A.M.G.S. synthesized the rosamine dye, F.G., J.M.P. and T.L.-C. analyzed the data and wrote the paper. All authors read and approved the manuscript.

Conflicts of Interest: The authors declare no conflict of interest.

References

1. Chen, X.; Pradhan, T.; Wang, F.; Kim, J.S.; Yoon, J. Fluorescent Chemosensors Based on Spiroring-Opening of Xanthenes and Related Derivatives. *Chem. Rev.* **2012**, *112*, 1910–1956.
2. Yang, P.; Wirnsberger, G.; Huanng, H.C.; Cordero, S.R.; McGehee, M.D.; Scott, B.; Deng, T.; Whitesides, G.M.; Cmelka, G.F.; Buratto, S.K.; et al. Mirrorless Lasing from Mesostructured Waveguides Patterned by Soft Lithography. *Science* **2000**, *287*, 465–467.
3. Sasai, R.; Iyi, N.; Fujita, T.; Arbeloa, F.L.; Martínez, V.M.; Takagi, K.; Itoh, H. Luminescence Properties of Rhodamine 6G Intercalated in Surfactant/Clay Hybrid Thin Solid Films. *Langmuir* **2004**, *20*, 4715–4719.
4. Marlow, F.; McGehee, M.D.; Zhao, D.; Chmelka, B.F.; Stucky, G.D. Doped Mesoporous Silica Fibers: A New Laser Material. *Adv. Mater.* **1999**, *11*, 632–636.

5. Tleugabulova, D.; Zhang, Z.; Chen, Y.; Brook, M.A.; Brennan, J.D. Fluorescence Anisotropy in Studies of Solute Interactions with Covalently Modified Colloidal Silica Nanoparticles. *Langmuir* **2004**, *20*, 848–854.
6. Bahadur, L.; Srivastava, P. Efficient Photon-to-Electron Conversion with Rhodamine 6G-sensitized Nanocrystalline n-ZnO Thin Film Electrodes in Acetonitrile Solution. *Sol. Energy Mater. Sol. Cells* **2003**, *79*, 235–248.
7. Aragay, G.; Pons, J.; Merkoçi, A. Recent Trends in Macro-, Micro-, and Nanomaterial-Based Tools and Strategies for Heavy-Metal Detection. *Chem. Rev.* **2011**, *111*, 3433–3458.
8. Kim, H.N.; Lee, M.H.; Kim, H.J.; Kim, J.S.; Yoon, J. A New Trend in Rhodamine-Based Chemosensors: Application of Spirolactam Ring-Opening to Sensing Ions. *Chem. Soc. Rev.* **2008**, *37*, 1465–1472.
9. Sánchez-Valencia, J.R.; Toudert, J.; González-García, L.; González-Elipe, A.R.; Barranco, A. Excitation Transfer Mechanism Along the Visible to the Near-IR in Rhodamine J-Heteroaggregates. *Chem. Commun.* **2010**, *46*, 4372–4374.
10. Sánchez-Valencia, J.R.; Blaszczyk-Lezak, I.; Espinós, J.P.; Hamad, S.; González-Elipe, A.R.; Barranco, A. Incorporation and Thermal Evolution of Rhodamine 6G Dye Molecules Adsorbed in Porous Columnar Optical SiO_2 Thin Films. *Langmuir* **2009**, *25*, 9140–9148.
11. Sánchez-Valencia, J.R.; Borrás, A.; Barranco, A.; Rico, V.J.; Espinós, J.P.; González-Elipe, A.R. Preillumination of TiO_2 and Ta_2O_5 Photoactive Thin Films As a Tool to Tailor the Synthesis of Composite Materials. *Langmuir* **2008**, *24*, 9460–9469.
12. Drexhage, K. Fluorescence Efficiency of Laser Dyes. *J. Res. Natl. Bur. Stand. A Phys. Chem.* **1976**, *80*, 421–428.
13. Beija, M.; Alfonso, C.A.M.; Martinho, J.M.G. Synthesis and Applications of Rhodamine Derivatives as Fluorescent Probes. *Chem. Soc. Rev.* **2009**, *38*, 2410–2433.
14. Sun, Y.Q.; Liu, J.; Lv, X.; Liu, Y.; Zhao, Y.; Guo, W. Rhodamine-inspired Far-red to Near-infrared Dyes and their Application as Fluorescence Probes. *Angew. Chem. Int. Ed.* **2012**, *51*, 7634–7636.
15. Koide, Y.; Kawaguchi, M.; Urano, Y.; Hanaoka, K.; Komatsu, T.; Abo, M.; Terai, T.; Nagano, T. A Reversible Near-infrared Fluorescence Probe for Reactive Oxygen Species based on Te-rhodamine. *Chem. Comm.* **2012**, *48*, 3091–3093.
16. Choi, J.Y.; Kim, W.; Yoon, J. Rhodamine Based Fluorescent Chemosensors for Hg^{2+} and its Biological Application. *Bull. Korean Chem. Soc.* **2012**, *33*, 2359–2364.
17. Niu, G.; Liu, W.; Zhou, B.; Xiao, H.; Zhang, H.; Wu, J.; Ge, J.; Wang, P. Deep-Red and Near-Infrared Xanthene Dyes for Rapid Live Cell Imaging. *J. Org. Chem.* **2016** *81*, 7393–7399.
18. Jeong, Y.; Yoon, J. Recent Progress on Fluorescent Chemosensors for Metal Ions. *Inorg. Chim. Acta* **2012**, *381*, 2–14.
19. Sivaraman, G.; Chellappa, D. Rhodamine Based Sensor for Naked-Eye Detection and Live Cell Imaging of Fluoride Ions. *J. Mater. Chem. B* **2013**, *1*, 5768–5772.
20. Corma, A.; Garcia, H. Silica-Bound Homogenous Catalysts as Recoverable and Reusable Catalysts in Organic Synthesis. *Adv. Synth. Catal.* **2006**, *348*, 1391–1412.
21. Taguchi, A.; Schuth, F. Ordered Mesoporous Materials in Catalysis. *Microporous Mesoporous Mater.* **2005**, *77*, 1–45.
22. Hartmann, M. Ordered Mesoporous Materials for Bioadsorption and Biocatalysis. *Chem. Mat.* **2005**, *17*, 4577–4593.
23. Germain, J.; Fréchet, J.M.J.; Svec, F. Nanoporous Polymers for Hydrogen Storage. *Small* **2009**, *5*, 1098–1111.
24. Czaja, A.U.; Trukhan, N.; Muller, U. Industrial Applications of Metal-Organic Frameworks. *Chem. Soc. Rev.* **2009**, *38*, 1284–1293.
25. Baskaran, S.; Liu, J.; Domansky, K.; Kohler, N.; Li, X.; Coyle, C.; Fryxell, G.E.; Thevuthasan, S.; Williford, R.E. Low Dielectric Constant Mesoporous Silica Films Through Molecularly Templated Synthesis. *Adv. Mater.* **2000**, *12*, 291–294.
26. Scott, B.J.; Wirnsberger, G.; Stucky, G.D. Mesoporous and Mesostructured Materials for Optical Applications. *Chem. Mater.* **2001**, *13*, 3140–3150.
27. Tam-Chang, S.W.; Huang, L. Chromonic Liquid Crystals: Properties and Applications as Functional Materials. *Chem. Commun*. **2008**, *17*, 1957–1967.
28. Van Esch, J.H.; Feringa, B.L. New Functional Materials Based on Self–Assembling Organogels: From Serendipity towards Design. *Angew. Chem. Int. Ed.* **2000**, *39*, 2263–2266.

29. Liu, X.D.; Esker, A.R.; Häußler, M.; Kim, C.; Lucas, P.; Matsunaga, M.; Nishi, N.; Robin, J.-J.; Tang, B.Z.; Wang, D.-A.; et al. *Functional Materials and Biomaterials*; Springer: Berlin/Heidelberg, Germany, 2007; pp. 149–178.
30. Abou Neel, E.A.; Pickup, D.M.; Valappil, S.P.; Newport, R.J.; Knowles, J.C. Bioactive Functional Materials: A Perspective on Phosphate-Based Glasses. *J. Mater. Chem.* **2009**, *19*, 690–701.
31. Bockstaller, M.R.; Mickiewicz, R.A.; Thomas, E.L. Block Copolymer Nanocomposites: Perspectives for Tailored Functional Materials. *Adv. Mater.* **2005**, *17*, 1331–1349.
32. Cohen, R.E. Block Copolymers as Templates for Functional Materials. *Curr. Opin. Solid State Mater. Sci.* **1999**, *4*, 587–590.
33. Matsukawa, K. Development of Photo-functional Materials from Organic/Inorganic Nano-Hybrids. *J. Photopolym. Sci. Technol.* **2005**, *18*, 203–210.
34. Yoon, K.B. Organization of Zeolite Microcrystals for Production of Functional Materials. *Acc. Chem. Res.* **2006**, *40*, 29–40.
35. Schöllhorn, R. Intercalation Systems as Nanostructured Functional Materials. *Chem. Mater.* **1996**, *8*, 1747–1757.
36. Fryxell, G.E. The Synthesis of Functional Mesoporous Materials. *Inorg. Chem. Commun.* **2006**, *9*, 1141–1150.
37. Yao, W.T.; Yu, S.H. Synthesis of Semiconducting Functional Materials in Solution: From II-VI Semiconductor to Inorganic–Organic Hybrid Semiconductor Nanomaterials. *Adv. Funct. Mater.* **2008**, *18*, 3357–3366.
38. Liu, P.S.; Liang, K.M. Review Functional Materials of Porous Metals Made by P/M, Electroplating and Some Other Techniques. *J. Mater. Sci.* **2001**, *36*, 5059–5072.
39. Powell, C.F.; Oxley, J.H.; Blocher, J.M. *Vapor Deposition*; John Wiley & Sons: New York, NY, USA, 1966.
40. Robbic, K.; Brett, M.J. Sculptured Thin Films and Glancing Angle Deposition: Growth Mechanics and Applications. *J. Vac. Sci. Technol. A* **1997**, *15*, 1460–1465.
41. Wang, S.; Xia, G.; He, H.; Yi, K.; Shao, J.; Fan, Z. First-Principles Study of Shear Deformation in TiAl Alloys. *J. Alloys Compd.* **2007**, *431*, 287–291.
42. Brett, M.J.; Hawkeye, M.M. New Materials at a Glance. *Science* **2008**, *319*, 1192–1193.
43. Kosmulski, M. *Chemical Properties of Material Surfaces*; Marcel Dekker: New York, NY, USA, 2001.
44. Hinckley, D.A.; Seybold, P.G. A Spectroscopic/Thermodynamic Study of the Rhodamine B Lactone ↔ Zwitterion Equilibrium. *Spectrochim. Acta* **1998**, *44A*, 1053–1059.
45. Cardoso, I.C.S.; Amorim, A.L.; Queirós, C.; Lopes, S.C.; Gameiro, P.; de Castro, B.; Rangel, M.; Silva, A.M.G. Microwave-Assisted Synthesis and Spectroscopic Properties of 4′-Substituted Rosamine Fluorophores and Naphthyl Analogues. *Eur. J. Org. Chem.* **2012**, *29*, 5810–5817.
46. U.S. Environmental Protection Agency. Air Trends Summary Report. Available online: http://www.epa.gov/oar/aqtrnd95/no2.html (accessed on 26 January 2017).
47. Mchedlov-Petrosyan, N.; Kholin, Y.V. Aggregation of Rhodamine B in Water. *Russ. J. Appl. Chem.* **2004**, *77*, 414–422.
48. Setiawan, D.; Kazaryan, A.; Martoprawirob, M.A.; Filatov, M. A First Principles Study of Fluorescence Quenching in Rhodamine B Dimers: How Can Quenching Occur in Dimeric Species? *Phys. Chem. Chem. Phys.* **2010**, *12*, 11238–11244.
49. Würth, C.; Grabolle, M.; Pauli, J.; Spieles, M.; Resch-Genger, U. Relative and Absolute Determination of Fluorescence Quantum Yields of Transparent Samples. *Nature* **2013**, *8*, 1535–1550.
50. Kasnavia, T.N.; Vu, D.; Sabatini, D.A. Fluorescent Dye and Media Properties Affecting Sorption and Tracer Selection. *Groundwater* **1999**, *37*, 376–381.
51. Hiemenz, P.C.; Rajagopalan, R. *Principles of Colloids and Surface Chemistry*; Marcel Dekker: New York, NY, USA, 1997.
52. Yariv, S.; Nasser, A.; Bar-On, P. Metachromasy in clay minerals. Spectroscopy study of the adsorption of crystal violet by Laponite. *J. Chem. Soc. Faraday Trans.* **1990**, *86*, 1593–1598.
53. Fujii, T.; Ishii, A.; Anpo, M. Absorption and Fluorescence Spectra of Rhodamine B molecules Encapsulated in Silica Gel Networks and their Thermal Stability. *J. Photochem. Photobiol. A Chem.* **1990**, *54*, 231–237.
54. Adamovich, L.P.; Mel'nik, V.V.; Mchedlov-Petrosyan, N.O. Rhodamine Equilibria in Water-Salt Solutions. *Zhurnal Fiz. Khimii* **1979**, *53*, 356–359.

55. De Miguel, G.; Pérez-Moales, M.; Martín-Romero, M.T.; Muñoz, E.; Richardson, T.H.; Camacho, L. Aggregation of a Water-Soluble Tetracationic Porphyrin in Mixed LB Films with a Calix[8]arene Carboxylic Acid Derivative. *Langmuir* **2007**, *23*, 3794–3801.
56. Özacar, M.; Senglil, I.A. Adsorption of Acid Dyes from Aqueous Solutions by Calcined Alunite and Granular Activated Carbon. *Adsorption* **2002**, *8*, 301–308.
57. Ho, Y.S. Adsorption of Heavy Metals from Waste Streams by Peat. Ph.D. Thesis, University of Brimmingham, Brimmingham, UK, 1995.
58. Watanabe, H.; Hayazawa, N.; Inouye, Y.; Kawata, S. DFT Vibrational Calculations of Rhodamine 6G Adsorbed on Silver: Analysis of Tip-Enhanced Raman Spectroscopy. *J. Phys. Chem. B* **2005**, *109*, 5012–5020.
59. Morterra, C. An Infrared Spectroscopic Study of Anatase Properties. Part 6—Surface Hydration and Strong Lewis Acidity of Pure and Sulphate-Doped Preparations. *Faraday Trans.* **1988**, *84*, 1617–1637.
60. Maira, A.J.; Coronado, J.M.; Augugliaro, V.; Yeung, K.L.; Conesa, J.C.; Soria, J. Fourier Transform Infrared Study of the Performance of Nanostructured TiO_2 Particles for the Photocatalytic Oxidation of Gaseous Toluene. *J. Catal.* **2001**, *202*, 413–420.
61. Isaienko, O.; Nihonyanagi, S.; Sil, D.; Borguet, E. Observation of the Bending Mode of Interfacial Water at Silica Surfaces by Near-Infrared Vibrational Sum-Frequency Generation Spectroscopy of the [Stretch+ Bend] Combination Bands. *J. Phys. Chem. Lett.* **2013**, *4*, 531–535.
62. López-Arbeloa, F.; Tapia-Estévez, M.J.; López-Arbeloa, T.; López-Arbeloa, I. Spectroscopic Study of the Adsorption of Rhodamine 6G on Clay Minerals in Aqueous Suspensions. *Clay Miner.* **1997**, *32*, 97–106.
63. Arbeloa, F.L.; Martínez, V.M.; López, T.A.; Arbeloa, I.L. Photoresponse and anisotropy of rhodamine dye intercalated in ordered layered films. *J. Photochem. Photobiol. C* **2007**, *8*, 85–108.
64. Tapia-Estévez, M.J.; López-Arbeloa, F.; López-Arbeloa, T.; López-Arbeloa, I.; Schoonheydt, R.A. Spectroscopic Study of the Adsorption of Rhodamine 6G on Laponite B for Low Loadings. *Clay Miner.* **1994**, *29*, 105–113.
65. Pedrosa, J.M.; Dooling, C.M.; Richardson, T.H.; Hyde, R.K.; Hunter, C.A.; Martín, M.T.; Camacho, L. The Optical Gas-Sensing Properties of an Asymmetrically Substituted Porphyrin. *J. Mater. Chem.* **2002**, *12*, 2659–2664.
66. Gulino, A.; Mineo, P.; Scamporrino, E.; Vitalini, D.; Fragalà, I.; Fragalà, I. Molecularly engineered silica surfaces with an assembled porphyrin monolayer as optical NO_2 molecular recognizers. *Chem. Mater.* **2004**, *16*, 1838–1840.
67. Gulino, A.; Bazzano, S.; Mineo, P.; Scamporrino, E.; Vitalini, D.; Fragalà, I.; Fragalà, I. Characterization, optical recognition behavior, sensitivity, and selectivity of silica surfaces functionalized with a porphyrin monolayer. *Chem. Mater.* **2005**, *17*, 521–526.
68. Pedrosa, J.M.; Dooling, C.M.; Richardson, T.H.; Hyde, R.K.; Hunter, C.A.; Martín, M.T.; Camacho, L. Influence of Molecular Organization of Asymmetrically Substituted Porphyrins on Their Response to NO_2 Gas. *Langmuir* **2002**, *18*, 7594–7601.
69. Roales, J.; Pedrosa, J.M.; Guillén, M.G.; Lopes-Costa, T.; Castillero, P.; Barranco, A.; González-Elipe, A.R. Free-Base Carboxyphenyl Porphyrin Films Using a TiO_2 Columnar Matrix: Characterization and Application as NO_2 Sensors. *Sensors* **2015**, *15*, 11118–11132.
70. Grauer, Z.; Avnir, D.; Yariv, S. Adsorption Characteristics of Rhodamine 6G on Montmorillonite and Laponite, Elucidated from Electronic Absorption and Emission Spectra. *Can. J. Chem.* **1984**, *62*, 1889–1984.
71. Castillero, P.; Sánchez-Valencia, J.R.; Cano, M.; Pedrosa, J.M.; Roales, J.; Barranco, A.; González-Elipe, A.R. Active and Optically Transparent Tetracationic Porphyrin/TiO_2 Composite Thin Films. *ACS Appl. Mater. Interfaces* **2010**, *2*, 712–721.
72. Roales, J.; Pedrosa, J.M.; Castillero, P.; Cano, M.; Richardson, T.H.; Barranco, Á.; González-Elipe, A.R. Selective Detection of Volatile Organic Compounds by Spectral Imaging of Porphyrin Derivatives Bound to TiO_2 Porous Films. *ACS Appl. Mater. Interfaces* **2012**, *4*, 5147–5154.